

Document downloaded from:

<http://hdl.handle.net/10251/194385>

This paper must be cited as:

Valencia Sullca, JF.; Cogollos, S.; Boria Esbert, VE.; Guglielmi, M. (2022). Compact Dual-Band and Wideband Filters With Resonant Apertures in Rectangular Waveguide. *IEEE Transactions on Microwave Theory and Techniques*. 70(6):3125-3140.
<https://doi.org/10.1109/TMTT.2022.3162307>



The final publication is available at

<https://doi.org/10.1109/TMTT.2022.3162307>

Copyright Institute of Electrical and Electronics Engineers

Additional Information

Compact Dual-Band and Wideband Filters With Resonant Apertures in Rectangular Waveguide

Joaquin F. Valencia Sullca, Santiago Cogollos, *Member, IEEE*, Vicente E. Boria, *Fellow, IEEE* and Marco Guglielmi, *Life Fellow, IEEE*

Abstract—The objective of this paper is to describe a new family of microwave bandpass filters in rectangular waveguide, based on resonant apertures, that can be used to implement both single and dual band transfer functions. The use of capacitive stubs and a staircase configuration is also discussed, in order to enhance the out-of-band response and the selectivity of the filter with respect to the state-of-the-art. Finally, simulations are compared with measured results, showing very good agreement, thereby fully validating both the new filter topologies and the design procedure.

Index Terms—Band-pass filters, capacitive irises, dual band, extended pass band, resonant apertures, staircase and stubs.

I. INTRODUCTION

MICROWAVE filters have always been the subject of very substantial research since the very early days of microwaves, and a very large number of publications can indeed be found in the technical literature discussing a wide variety of filter structures and design techniques (see [1], [2] for excellent reviews). Many different technologies can be used to implement microwave filters, common examples are coaxial, planar, or metallic waveguide technology ([3], [4]), to mention a few. Filters are normally designed to satisfy a set of requirements in their electrical performance, both in-band and out-of-band. In particular, the filter bandwidth and the extent of the spurious-free out-of-band performance are among the most important parameters in the design of microwave filters.

It is interesting to note that many examples of filters with a wide pass band have indeed been discussed in planar technology. For instance, a novel ultra-wideband (UWB) bandpass filter (BPF) which uses a hybrid microstrip and coplanar waveguide (CPW) structure was proposed in [5]. Also, a compact ultra-wideband bandpass filter, based on a microstrip and coplanar waveguide (CPW) structure, has been proposed in [6]. However, these structures have high insertion loss, limited out-of-band rejection at high frequencies, and low power handling capabilities.

On the other hand, wide pass band microwave filters implemented in rectangular waveguide technology typically have

This work was supported by the Ministerio de Ciencia e Innovación, Spanish Government, through the Research and Development Project PID2019-103982RB under Grant MCIN/AEI/10.13039/501100011033, and by Generalitat Valenciana under Santiago Grisolía grant GRISOLIA/2017/073. This paper is an expanded version from the IEEE MTT-S International Microwave Symposium (IMS 2021), Atlanta, GA, USA, June 20-25, 2021.

J.F. Valencia Sulca, S. Cogollos, V.E. Boria and M. Guglielmi, are with the Departamento de Comunicaciones, iTEAM Group, Universitat Politècnica de València, E-46022 Valencia, Spain (e-mails: joavasu2@teleco.upv.es, sancobo@dcom.upv.es, vboria@dcom.upv.es, marco.guglielmi@iteam.upv.es).

low insertion loss and high power handling capabilities. In [7], for instance, a wide band filter has been designed with a good out-of-band performance, and a wide rejection band. However, the resulting filter structure is rather long, since it is a cascade of an inductive bandpass filter and a capacitive low pass filter. Traditionally, the most common implementation of band-pass filters in rectangular waveguide technology has been based on inductive irises [8]. For narrow band applications, inductive filters have excellent high power capabilities and very good selectivity. However, the out-of-band performance may be strongly degraded for wide band applications. In [9]–[11], for instance, waveguide filters based on inductive irises have been designed for narrow to fairly wide bandwidth applications. More recently, several techniques have been discussed to improve the out-of-band performance of inductive filters. In [12], a new technique has been proposed, using a particular arrangement of the coupling windows, in order to improve the out-of-band response. However, this approach has been demonstrated only for narrow-band applications.

A well known alternative solution, to improve the out-of-band performance, is the use of capacitive irises in band pass filters, as shown in [13] and [14]. Capacitive band pass filters can, in fact, provide a wide spurious-free region above the pass band. However, the use of capacitive structures may also introduce problems, such as the appearance of resonances below the filter pass band, and high power limitations.

More recently, several papers have discussed the combined use of capacitive and inductive irises in band pass filters [15] and [16]. Using both capacitive and inductive irises can, in fact, improve the out-of-band performance and obtain, at the same time, wide-band waveguide filters. However, in some cases, this happens at the cost of reduced filter selectivity.

A well-known technique that allows to improve both the out-of-band performance and the filter selectivity is the introduction of transmission zeros (TZs). For instance, an approach in rectangular waveguide has also been proposed in [17], where a new capacitive obstacle has been added to the structure of filter, in order to introduce TZs in a wide frequency range.

In this context, a recent contribution can be found in the technical literature that discusses how to improve the out-of-band performance and selectivity of a microwave wide-band filter using a staircase configuration with E-plane T-junctions and shorted stubs, as shown in [18] and [19]. However, even though the structure proposed does produce an important improvement of the out-of-band response and a good enhancement of the filter selectivity, it can result in

rather long structures for high order filters.

Furthermore, there are also many papers in the technical literature that use capacitive irises both as resonators and as extracted poles. For instance, an asymmetric-iris coupled-cavity filter has been proposed in [20], where the interference between modes is used to improve the out-of-band response. Moreover, further implementations have been proposed to design rectangular waveguide structures which are coupled by rectangular iris loaded E- or H-plane T-junctions [21] and [22].

Compact in-line pseudo-elliptic filters were proposed in [23], which are based on the combination of resonant irises with other resonances, such as the TE_{101} and TM_{110} rectangular waveguide cavity modes. An additional approach is discussed in [24] for a compact in-line pseudo-elliptic filter based on the TM_{110} mode cavity that can achieve wide stop bands by carefully selecting the coupling irises. Furthermore, a new class of broadband pseudo-highpass waveguide filters based on the TM_{101} mode and iris resonances has been proposed in [25].

Yet another possibility to design filters in rectangular waveguide is to use resonant apertures (RAs) [26]. For instance, evanescent mode filters have been implemented in [27] and [28], where direct-coupled resonant apertures have been used to extend the rejection performance and reduce the total length of the filter. More recently, a contribution has shown how the low insertion loss and high return loss of an evanescent mode filter can be improved by using, at the same time, a below cut-off rectangular waveguide and capacitive irises in the resonant cavities of the filter [29].

Many additional examples of the use of resonant irises can also be found in the technical literature for wide band filters in rectangular waveguide technology. In [30] and [31], for instance, wide band band-pass filters with high selectivity have been proposed, which use resonant irises as filter resonators. Also, a directly coupled non-centered resonant irises filter has been designed in [32], in order to provide a broadband and highly selective response in Ka band, with a good spurious-free range. Another example of the use of resonant irises as resonators of a microwave bandpass filter is found in [33]. More recently, a contribution has shown preliminary results on how to design dual-band waveguide filters using resonant apertures (RAs), with an important improvement of the out-of-band performance and selectivity by using, at the same time, capacitive stubs and a staircase configuration [34].

In this context, therefore, the objective of this paper is to significantly extend the results presented in [34]. In particular, the additional topics discussed with respect to [34] are:

- 1) A parametric analysis of the basic RA with the objective of demonstrating how input coupling, output coupling and resonance frequency can be controlled independently.
- 2) The systematic design procedures of dual band and wide band filters, showing good performance with a structure that is easy to manufacture.
- 3) A sensitivity analysis to identify the most appropriate manufacturing process.
- 4) The high power analysis of the hardware in order to identify the power level at which multiplication is

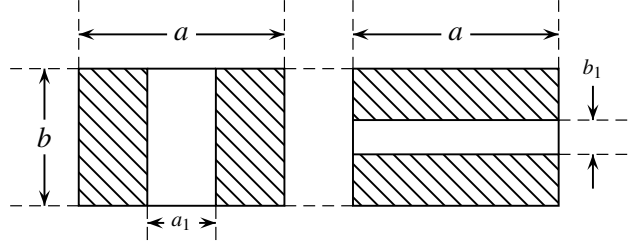


Fig. 1. Typical irises in a rectangular waveguide (front view). Left: centered inductive iris of width a_1 . Right: centered capacitive iris of height b_1 .

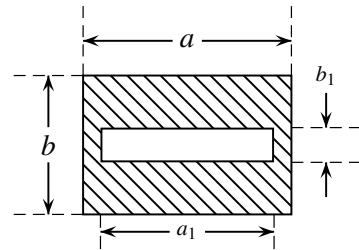


Fig. 2. Resonant aperture in a rectangular waveguide (front view). The aperture is centered and has width a_1 and height b_1 .

initiated.

Finally, in addition to theory, measured results are also discussed, showing excellent agreement with simulations, thereby fully validating the new filter topologies that we propose.

II. BASIC RESONANT APERTURE

As it is well known, the design of classic inductive and/or capacitive microwave filters can be based on half-wavelength resonators that are coupled to each other by thick inductive and/or capacitive irises (see Fig. 1). It is also well known that inductive and capacitive irises can be considered to be essentially equivalent to a shunt inductor or capacitor, respectively [35]. In this paper, however, we will use RAs which exhibit, in a single aperture, both capacitive and inductive behaviors. They can therefore be represented as a shunt combination of an inductor and a capacitor. This parallel combination will then be the main resonant structure of our filters. Fig. 2 shows the structure of the basic resonant aperture that we propose to use in the remainder of this paper. Fig. 3 shows the top and side views of Fig. 2, where we can define the dimensions of the waveguide to the left of the RA (a and b), the dimensions of the resonant aperture (a_1 , b_1 and t) and the dimensions of the waveguide to the right of the RA (w and h).

To better understand the behavior of a resonant aperture, we now perform a parametric study. The starting point is a centered capacitive aperture in a WR-90 waveguide. The aperture is $a_1 = 22.86$ mm wide, $b_1 = 3.5$ mm high and $t = 2.0$ mm thick.

The first parameter that we change is a_1 . Fig. 4 shows the effect of changing a_1 from 22.86 mm to 13.00 mm. It is interesting to observe that the resonance for $a_1 = 22.86$ mm is essentially the cutoff of the WR-90 waveguide. As the a_1 dimension decreases, the resonance of the aperture goes from

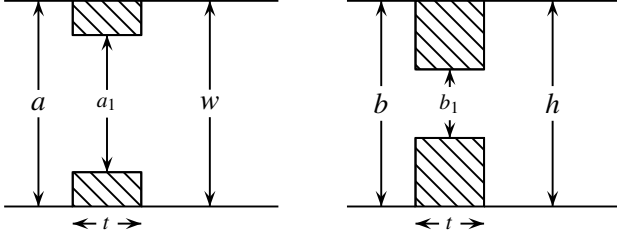


Fig. 3. Resonant aperture in a rectangular waveguide. Left: centered resonant aperture of width a_1 (top view). Right: centered resonant aperture of height b_1 (side view).

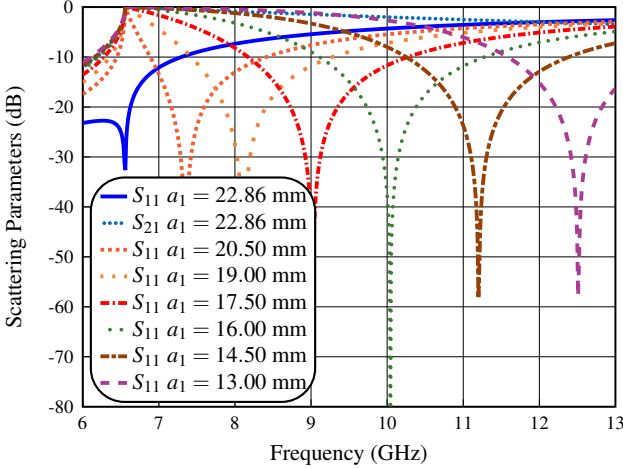


Fig. 4. Simulated performance of the resonant aperture, changing a_1 from 22.86 mm to 13.00 mm.

6.5 GHz to 12.4 GHz, which covers the standard operational bandwidth of the WR-90 waveguide (8.2 to 12.4 GHz).

The second parameter that we change is the height h of the waveguides connected to the right of the RA (see Fig. 3), while keeping the width of the RA constant ($a_1 = 21.50$ mm). In order to see the effect on the coupling while changing the height of the waveguide connected to the RA, first we study a symmetric structure, that is, we will keep $b = h$ throughout the experiment. Fig. 5 shows the effect of changing h from 10.16 mm to 7.50 mm. As we can see, decreasing the height of the waveguides connected to the RA, increases the resonant bandwidth. This is equivalent to increasing the coupling between the RA and the adjacent waveguides. It is also evident that the RA changes its resonance due to the loading effect of the waveguides.

Our real structure, however, will have different waveguides connected to the RAs. In the next experiment, therefore, we keep $b = 10.16$ mm, and change h from 10.16 mm to 13.50 mm (with the value of $a_1 = 20.00$ mm). The results obtained in this second experiment are shown in Fig. 6. As expected, increasing the height of the waveguide to the right of the RA, decreases the resonant bandwidth. This is equivalent to decreasing the coupling between the RA and the waveguide to the right. As a consequence, the return loss is no longer equal to ∞ , as it is the case when the input and output couplings have the same strength.

The third parameter that we change is the height b_1 of the

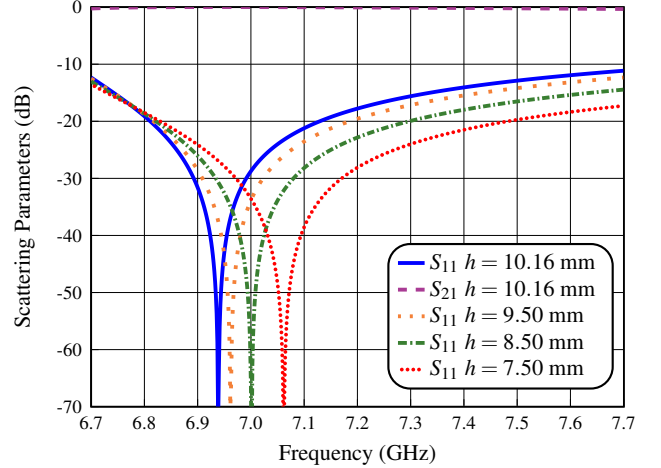


Fig. 5. Simulated performance of the resonant aperture, changing h from 10.16 mm to 7.50 mm. Here, $b = h$ for all simulations.

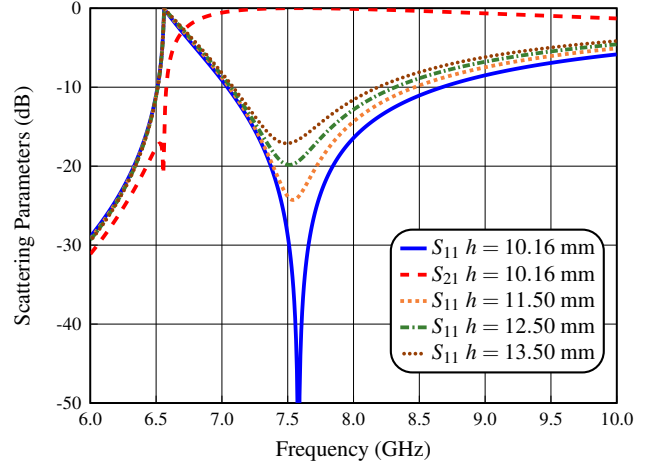


Fig. 6. Simulated performance of the resonant aperture, changing h from 10.16 mm to 13.50 mm. Here, $b = 10.16$ mm for all simulations.

RA, while keeping constant the value of $a_1 = 20.00$ mm and $h = 12.50$ mm, respectively. Fig. 7 shows the effect of changing b_1 from 3.5 mm to 2.0 mm, in steps of 0.5 mm. As we can see, decreasing the aperture height reduces the resonant bandwidth, and lowers the resonant frequency.

Finally, the last parameter that we change is the thickness t of the RA, while keeping constant the values of $a_1 = 20.00$ mm, $h = 12.50$ mm and $b_1 = 2.0$ mm. Fig. 8 shows the effect of decreasing the thickness from 2.0 to 0.5 mm, in steps of 0.5 mm. As we can see, decreasing t has an effect that is similar to increasing b_1 . However, the effect is not as strong.

Having explored the parametric behavior of the basic RA, we can conclude that we do have independent control of the three parameters of interest for filter design, namely, the resonant frequency, the input coupling and the output coupling. We are therefore ready to start the design of our filter.

It is important to note at this point that, in the response of a standard capacitive filter in rectangular waveguide, there is always a pass band near the cutoff of the rectangular waveguide (see [34]). This pass band is there because each of the capacitive irises is, as we have shown, a (lumped element)

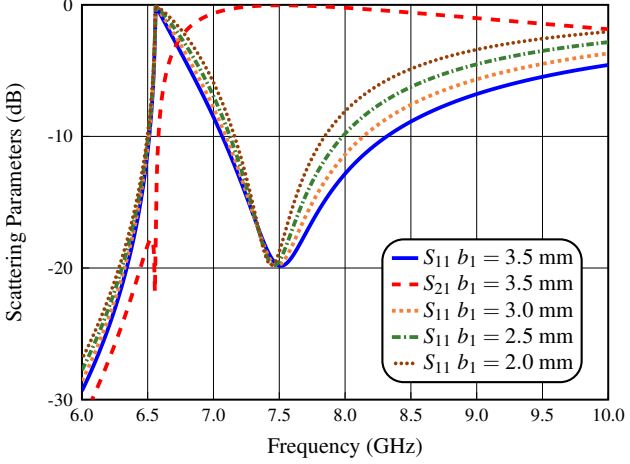


Fig. 7. Simulated performance of the resonant aperture, changing b_1 from 3.5 mm to 2.0 mm.

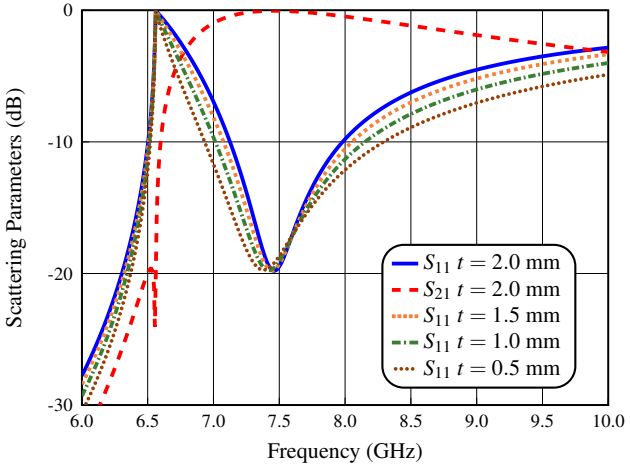


Fig. 8. Simulated performance of the resonant aperture, changing t from 2.0 mm to 0.5 mm.

resonator at the cutoff frequency. In a standard capacitive filter, at the cutoff frequency, the capacitive irises are coupled to each other by the length of waveguide between them (the distributed resonators) so that the structure behaves like *another* filter. This is, in fact, the origin of the spurious response that we observe near the cutoff. Increasing the frequency above cutoff, the capacitive iris becomes a shunt capacitance and behaves like an inverter. The length of waveguide between the capacitive apertures are now above cutoff and behave like standard distributed resonators.

Our idea is to exploit the resonant behavior of the capacitive irises by slightly shifting their resonance, thus transforming them from capacitive to resonant. We can then design filters where the resonance of the irises are shaping a lower pass band (the spurious band near cutoff) in addition to the upper band (where the waveguide sections resonate). With this in mind, two possibilities can be explored, namely, dual-band filters, and wide pass band filters based on RAs where the two bands are merged into one extended band.

III. DUAL BAND RA FILTER

We first explore the use of RAs to implement dual band filters. The design procedure that we propose is as follows:

- 1) For the lower band, we first design the normalized lumped element low pass network (g_i values) of the Chebyshev filter from the specifications of the return loss (RL), and the order $N + 1$.
- 2) We then design the band pass network composed of series and shunt resonators. The series resonators are then transformed into shunt resonators using admittance inverters $J_{i,i+1}, i = 0, \dots, N + 1$, with the following values

$$J_{0,1} = \sqrt{\frac{G_A \mathcal{W}_\lambda \mathcal{B}_1}{g_0 g_1}} \quad (1a)$$

$$J_{i,i+1} = \mathcal{W}_\lambda \sqrt{\frac{\mathcal{B}_i \mathcal{B}_{i+1}}{g_i g_{i+1}}}, \quad i = 1, \dots, N \quad (1b)$$

$$J_{N+1,N+2} = \sqrt{\frac{G_B \mathcal{W}_\lambda \mathcal{B}_{N+1}}{g_{N+1} g_{N+2}}} \quad (1c)$$

where G_A and G_B are the conductance in the input and output of the filter, \mathcal{W}_λ is the guided-wavelength bandwidth and \mathcal{B}_i is the susceptance slope parameter. This susceptance is chosen (because of the degree of freedom) in such a way that the inverter values given by (1) are close to the Y_0 of the standard waveguide at f_1 (center frequency of the lower band).

- 3) The admittance inverters are then transformed into quarter-wavelength waveguides, where the length of each resonator is $l_i(f_1) \approx \lambda_1/4$, where f_1 is the center frequency of the lower band. With this last step, we finally obtain the first band (lower band).
- 4) For the upper band, we first design a filter of order N with half-wavelength (distributed) resonators and $N + 1$ capacitive irises, where the length of each resonator is $l_i(f_2) \approx \lambda_2/2$, where f_2 is the center frequency of the upper band. The dimensions of the waveguides are initially chosen to obtain a characteristic admittance at f_1 equal to the inverter values obtained. This filter has its pass-band at the upper band of the intended dual-band design.
- 5) We now have the equivalent circuit model (see Fig. 9) and the basic dual-band structure. We can, therefore, optimize the performance of both bands simultaneously using this distributed model for a faster optimization process. The results are a good approximation for the initial point of the EM optimizer where the lumped resonators are substituted by RAs. We can now proceed with a final refinement in the filter performance. This is indeed possible because we do have the needed degrees of freedom, namely, a_1 , b_1 and the thickness (t) of each RA, plus the w , h and l dimensions of each distributed resonator.

With the procedure just described, we can easily obtain a pass band of order $N + 1$ at the lower frequency, due to the $N + 1$ RAs, and the second pass band of order N at the upper frequency, due to the N half-wavelength resonators.

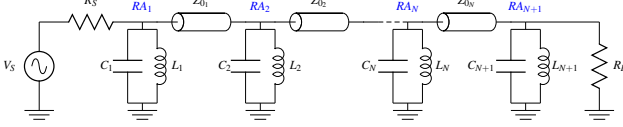


Fig. 9. Circuit model of the dual band RA filter.

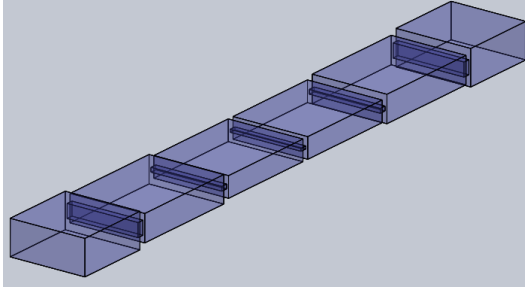


Fig. 10. Structure of the dual band RA filter.

Fig. 10 shows the structure of the proposed dual band RA filter, which has been obtained following the design procedure just described. Fig. 11 shows the simulated behavior of the structure of Fig. 10 (DB RA Filter), where the center frequencies are $f_1 = 7.42$ GHz and $f_2 = 10$ GHz, and the bandwidth of the two passbands are $BW_1 = 850$ MHz and $BW_2 = 1000$ MHz, respectively.

The performance shown in Fig. 11 has been obtained with the commercial tool FEST3D (v.2021 by AuroraSAT, now with Dassault Systèmes).

A. Capacitive Stubs

The dual band filter we just designed, has a shallow rejection level between the two pass bands. To improve this feature, we propose to use capacitive stubs in order to introduce transmissions zeros (TZs). Fig. 12 shows the basic stub geometry. Fig. 13 shows the structure of the dual band RA filter with two capacitive stubs before the input and output RAs (four stubs in total). Fig. 14 shows the simulated behavior of the structure in Fig. 13 (DB RA TZ Filter).

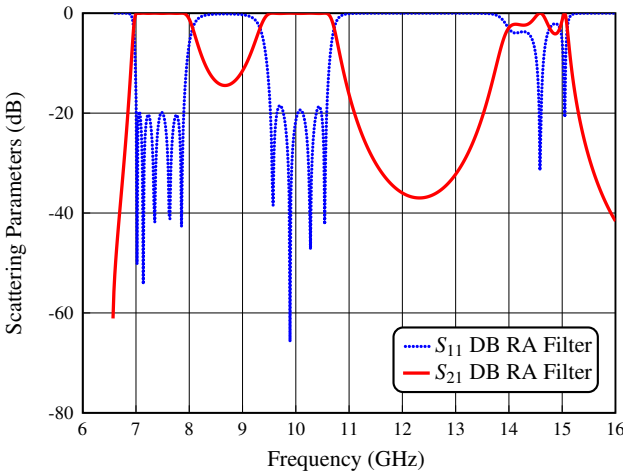


Fig. 11. Simulated performance of the dual band RA filter (DB RA Filter).

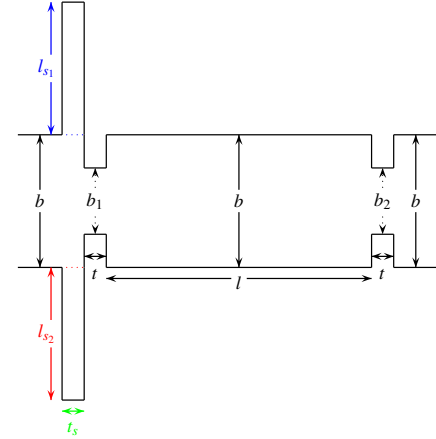


Fig. 12. Geometry of a resonator coupled with capacitive couplings in the front and end walls, and capacitive stubs (l_{s1} and l_{s2}) in the input of the resonator (side view).

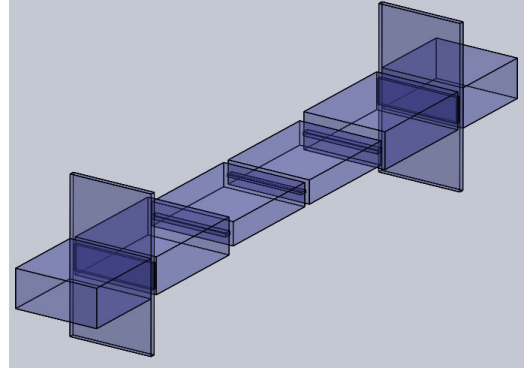


Fig. 13. Structure of the dual band RA filter with capacitive stubs before the input and output RAs.

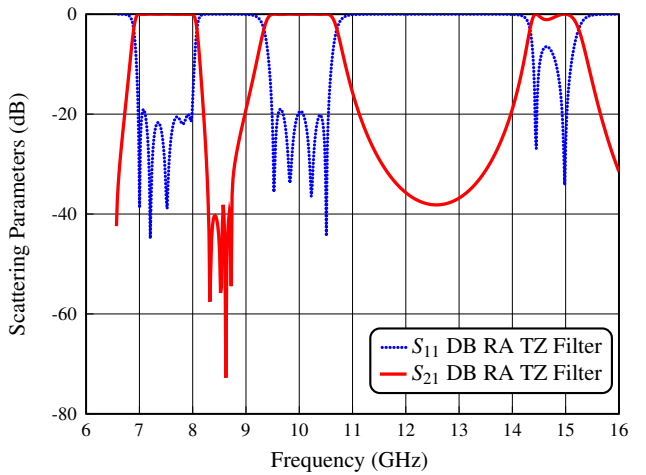


Fig. 14. Simulated performance of the dual band RA filter with capacitive stubs before the input and output RAs (DB RA TZ Filter).

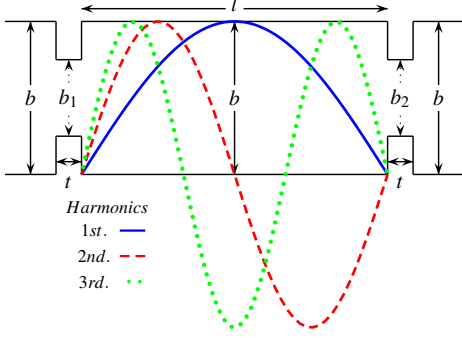


Fig. 15. Geometry of a resonator coupled with capacitive couplings in the front and end walls, with the first three resonant modes of a rectangular waveguide cavity (side view).

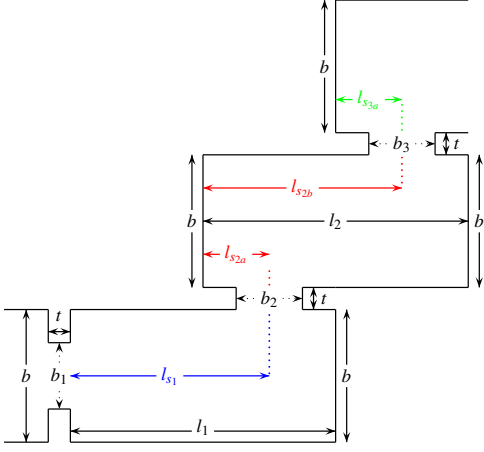


Fig. 16. Geometry of the three-resonator of the staircase configuration with the capacitive coupling apertures located at $l_{s1} = 3l_1/4$, $l_{s2a} = l_2/4$, $l_{s2b} = 3l_2/4$ and $l_{s3a} = l_3/4$ respectively, from the resonator input.

As we can see, the use of capacitive stubs has introduced four TZs, at 8.32, 8.52, 8.62 and 8.72 GHz, respectively, thereby significantly improving the rejection between the two pass bands of the filter. In addition, the resulting filter is rather compact for a nine-pole structure.

B. Staircase Filter

In this section, we propose an additional possibility for the improvement the out-of-band performance of our filter. This is essentially based on the implementation of the staircase configuration, similarly to what was discussed in [18] and [19]. To better clarify this concept, we show in Fig. 15 the electric field distribution of the first three resonant modes of a rectangular waveguide cavity of width a , height b and length l , in a resonator coupled with capacitive irises.

If we locate the capacitive irises at $l_s = 3l/4$ in Fig. 15, we can indeed obtain a very significant reduction of the coupling between higher order resonances and, as a consequence, improve the out-of-band response of the filter. Fig. 16 shows the basic staircase configuration.

One important feature of the basic dual-band filter in Fig. 10 is that, although we have a total of nine poles, the spurious response at approximately 14.5 GHz in Fig. 11 is

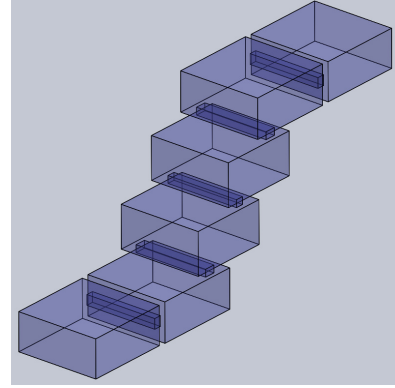


Fig. 17. Structure of the dual band RA staircase filter.

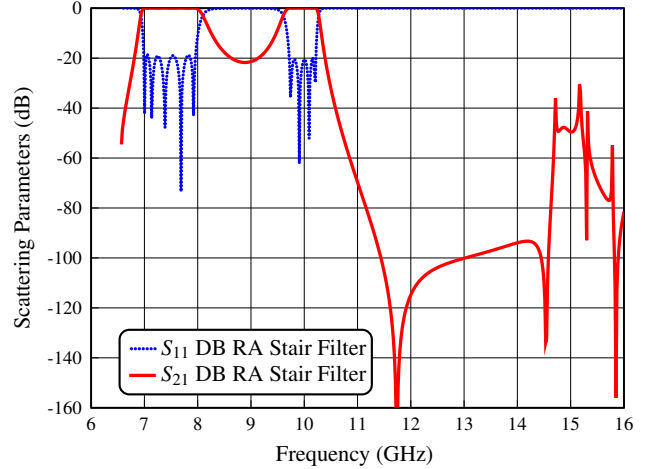


Fig. 18. Simulated performance of the dual band RA staircase (DB RA Stair Filter).

only due to the four distributed resonators, since the RAs behave basically as lumped elements resonators. However, this spurious response can be very effectively reduced with the help of the staircase configuration, as shown in [18] and [19].

Fig. 17 shows the structure of the dual band RA staircase filter. Fig. 18 shows the simulated behavior of the structure of Fig. 17 (DB RA Stair Filter).

As we can see, the use of this simple staircase structure results into a significant reduction and attenuation of the harmonics, with spurious response below -40 dB, and spikes reaching -35 and -30 dB at 14.71 and 15.16 GHz, respectively.

C. Staircase Filter with TZs

To further improve the out-of-band response of the dual band RA staircase filter, we now use capacitive stubs before the input and output RAs, and optimize the widths of the distributed resonator, as shown in Fig. 19. As already discussed, the location of the RAs along the resonators has been optimized to produce the maximum spurious rejection.

It is important to mention that a similar structure has already been discussed in [34]. The filter in Fig. 19 (DB RA Stair TZ Filter) is, however, a completely new structure that has been designed with wider, symmetric capacitive stubs, to

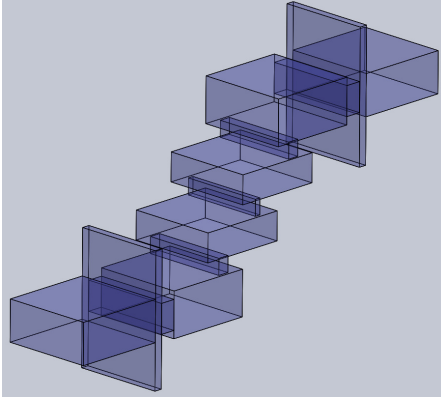


Fig. 19. Structure of the dual band RA staircase filter with capacitive stubs before the input and output RAs.

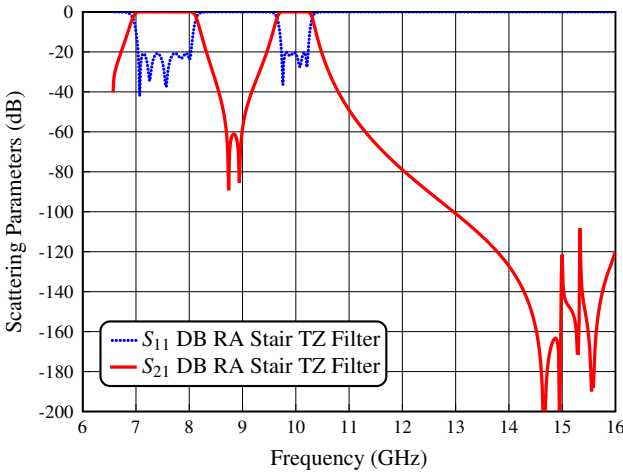


Fig. 20. Simulated performance of the dual band RA staircase filter with capacitive stubs before the input and output RAs (DB RA Stair TZ Filter).

further simplify the manufacturing process. Fig. 20 shows the resulting simulated performance.

As we can see, the resulting structure shows a significant reduction and attenuation of the harmonics, with spurious response below -120 dB and a spike reaching -108.0 dB at 15.32 GHz. Also, we can clearly see that there is now a strong rejection between the bands (below -60 dB) due to the two TZs at 8.72 and 8.95 GHz, respectively.

IV. EXTENDED BAND PASS RA FILTER

RA structures can also be used for designing extended band pass filters. What we need to do is to eliminate the rejection band between the two band-pass of the dual band RA filter. If we do that, we will, in fact, obtain a single wide band pass filter structure. Table I shows the electrical specification that we used for the extended band pass RA filter design.

The method that we propose to design an extended band pass RA filter is as follows:

First of all, the specifications shown in Table I are used to obtain the normalized lumped element low pass network of the filter (Chebyshev response). Specifically, we will obtain the g_i values from the specifications of the return loss (RL), and the

TABLE I
ELECTRICAL SPECIFICATIONS FOR THE REFERENCE FILTER.

Parameter	Requirement
Bandwidth	$BW = 1400 \text{ MHZ}$
In-band return loss	$RL > 20 \text{ dB}$
Center frequency	$f_0 = 7.55 \text{ GHz}$
Guide-wavelength fractional bandwidth	$\mathcal{W}_\lambda = 105.041 \text{ \%}$
Waveguide WR-90	$a = 22.86 \text{ mm}$ $b = 10.16 \text{ mm}$

order of the filter. In the low pass network, the series g_i values are inductors (L_n), and the shunt g_i values are capacitors (C_n). The first element (g_1 value) will be implemented with a shunt capacitor.

Once the lumped low pass model is built, a low-pass to band-pass transformation must be performed. The series inductors are transformed into series resonant circuits with the following values:

$$L_{ri} = \frac{L_n}{\Delta\omega} \quad (2)$$

$$C_{ri} = \frac{\Delta\omega}{L_n \omega_0^2} \quad (3)$$

The shunt capacitors are transformed into shunt resonant circuits with the following values:

$$L_i = \frac{\Delta\omega}{C_n \omega_0^2} \quad (4)$$

$$C_i = \frac{C_n}{\Delta\omega} \quad (5)$$

where $\Delta\omega$ corresponds to $2\pi BW$. Before computing the real values of the components of the band-pass filter, an impedance Z_0 must be chosen for de-normalizing the model. At this point, we want to transform the de-normalized lumped element model (Fig. 21) into a distributed band-pass filter of order $2N + 1$. To do that, we will implement the shunt resonators ($N + 1$) with RAs, and the series resonators (N) with half-wavelength waveguide resonators.

In order to obtain the distributed band pass model, the slope parameter, the guided wavelength and the characteristic impedance of each series resonator must be calculated. An LC series resonator has a slope parameter given by:

$$\chi_{ri} = \omega_0 L_{ri} \quad (6)$$

The guided wavelength expression is:

$$\lambda_g = \frac{\lambda_0}{\sqrt{1 - \left(\frac{f_c}{f_0}\right)^2}} \quad (7)$$

where $\lambda_0 = c/f$, $f_c = c/2a$. The relation between the slope parameter and the characteristic impedance of each waveguide is defined by the following expression [8]:

$$\chi_{ri} = Z_{0i} \frac{\pi}{2} \left(\frac{\lambda_{gi}}{\lambda_0} \right)^2 \quad (8)$$

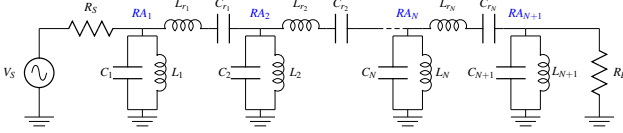


Fig. 21. Circuit model of the extended band pass RA filter.

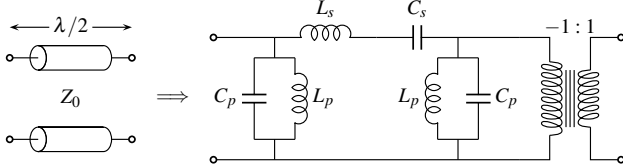


Fig. 22. Circuital model based on a PI configuration.

All these parameters are used to obtain the dimensions (a , b and length) of the waveguides that will replace the series resonators. Since we know the values of the characteristic impedance thanks to (8), we can obtain the relation between the dimensions a and b (b/a) of each waveguide using the following expression:

$$Z_{0i} = 2 \frac{b}{a} Z_{TE} \quad (9)$$

where Z_{TE} is the frequency dependent modal impedance of the fundamental mode. Since we know the dimensions a , b and length of the half-wavelength waveguide, we proceed to substitute the series resonators with real waveguide sections. To continue, we note that a half-wavelength waveguide can be modeled near the resonance frequency as a PI structure which is formed by one series and two shunt resonators, as shown in Fig. 22. The values of the lumped elements can then be obtained using the following expressions [36]:

$$L_s = \frac{\pi Z_0}{2 \omega_0} \quad (10)$$

$$C_s = \frac{2 Y_0}{\pi \omega_0} \quad (11)$$

$$C_p = \frac{\pi Y_0}{4 \omega_0} \quad (12)$$

$$L_p = \frac{4 Z_0}{\pi \omega_0} \quad (13)$$

The series part of the PI structure is our series resonator (L_{ri} and C_{ri}). We can then use (2) and (3) to solve for the characteristic impedance. The parasitic capacitance and inductance in parallel change the behavior of the original de-normalized C_i and L_i (shunt resonators). For this reason, it is compulsory to design new shunt resonators whose responses must be as similar as possible to the original ones (C_i and L_i), while including the parasitic effects. These new shunt resonators provide the responses needed to create the resonant apertures. So, after the distributed band pass model is defined, a fast optimization is enough to obtain the desired response. In this context, the variables available for the optimization are: the width, the height and the thickness (a_1 , b_1 and t) of each

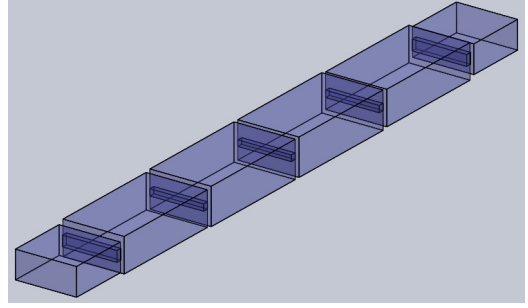


Fig. 23. Structure of the extended band pass RA filter.

RA, and the width, the height and the length (w , h , l) of each waveguide section.

A. Staircase Filter with TZs

Using the method just described, we have obtained the structure of the in-line extended band pass RA filter that is shown in Fig. 23.

As already mentioned, a further improvement of the out-of-band performance can be obtained by implementing both capacitive stubs and the staircase configuration. This will improve both the filter selectivity and its corresponding out-of-band response. Fig. 24 shows the structure of the extended band pass RA staircase filter with two stubs before and after the input and output RAs (EB RA Stair TZ Filter).

It is important to recall now that the TZs are due to a disruptive interference caused by the stubs. The capacitive stubs can, in fact, be viewed as a reactance in series with the transmission line representing the fundamental mode of the basic rectangular waveguide used for the filter. This reactance, however, is also the input impedance of the length of waveguide used to implement the capacitive stub. As a consequence, a transmission zero is introduced when the input impedance of the stub is equal to infinity. This corresponds to the frequency at which the stub is a quarter wavelength long. The frequency of the TZ can therefore be adjusted very easily by selecting the desired length.

Fig. 25 shows a comparison of the simulated behavior of the structures of Fig. 23 (EB RA Filter I) and Fig. 24 (EB RA Filter II) from 6.5 to 13 GHz.

As we can see in Fig. 25, the EB RA Filter I has a number of interesting features. First of all, the filter is a nine-pole filter, but it only has four distributed resonators. In fact, following our approach, we obtain a filter of order $2N + 1$, with $N + 1$ RAs and N distributed resonators. Furthermore, the spurious response of the filter is only due to the four distributed resonators, since the other five poles come from lumped element resonators. It is now important to note that, the EB RA Filter I shows spurious responses at 10.0 and 12.5 GHz, where the TE_{102} and TE_{103} modes are excited, respectively.

However, for the new EB RA Filter II, we now have spurious responses below -60 dB from 8.76 to 12.30 GHz, -40 dB from 12.30 to 13 GHz with spikes of -16.5, -8.36 and -26.33 dB at 12.32, 12.58 and 12.80 GHz, respectively.

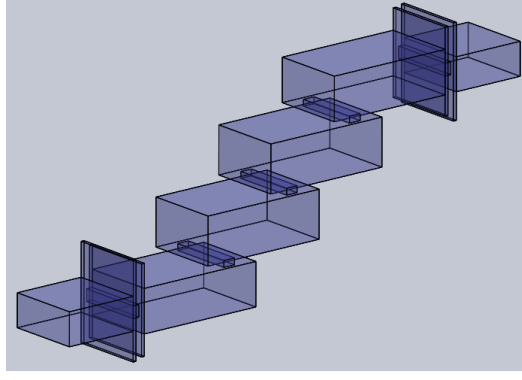


Fig. 24. Structure of the extended band pass RA staircase filter with two stubs both before and after of the input and output RAs.

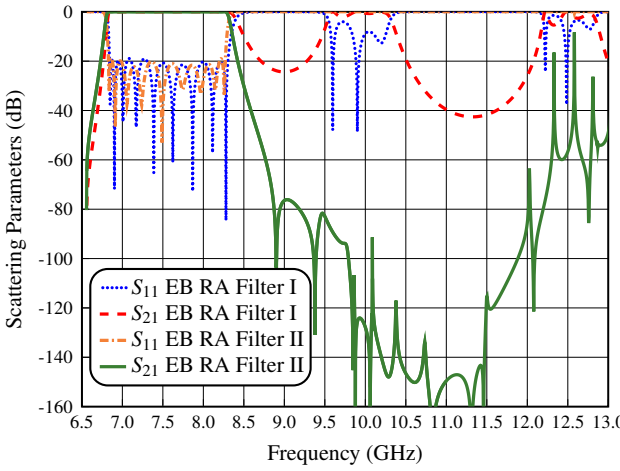


Fig. 25. Simulated performance of the EB RA Filter (EB RA Filter I), and the EB RA Stair TZ Filter (EB RA Filter II).

We can therefore conclude that combining capacitive stubs and the staircase configuration in the filter, results into an important improvement in the out-of-band response with attenuation and reduction of the spurious peaks and enhancement, at the same time, of the filter selectivity.

V. THE PROTOTYPES

The RA filtering structures that we have designed and simulated so far, have been designed with the commercial tool FEST3D in the high accuracy mode. It is important to mention that we have included in the simulations up to 120 accessible modes to connect discontinuities, and up to 3600 localized modes for their characterization, in both the dual band RA filter and extended band pass RA filter, respectively [37]. As a verification before manufacturing, we have also simulated the same structures with the full-wave electromagnetic simulator simulator CST (v.2021, CST GmbH, now with Dassault Systèmes).

A. Dual Band RA Prototype

The specifications of the dual band RA filter are as follows: for the lower band, the center frequency is $f_1 = 7.5$ GHz, the bandwidth is $BW_1 = 1000$ MHz and the in-band return loss is

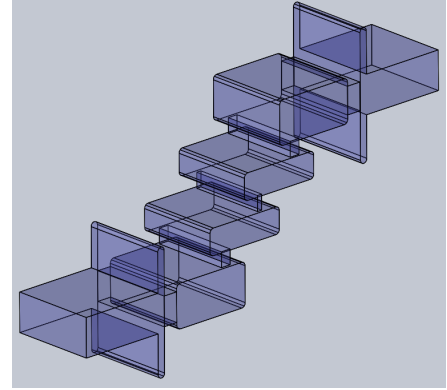


Fig. 26. Structure of the dual band RA staircase filter with capacitive stubs before the input and output RAs (DB RA Stair TZ Filter) designed with radius equal to $r_1 = 1.1$ mm in the distributed resonators and $r_2 = 1.0$ mm in the capacitive stubs, respectively.

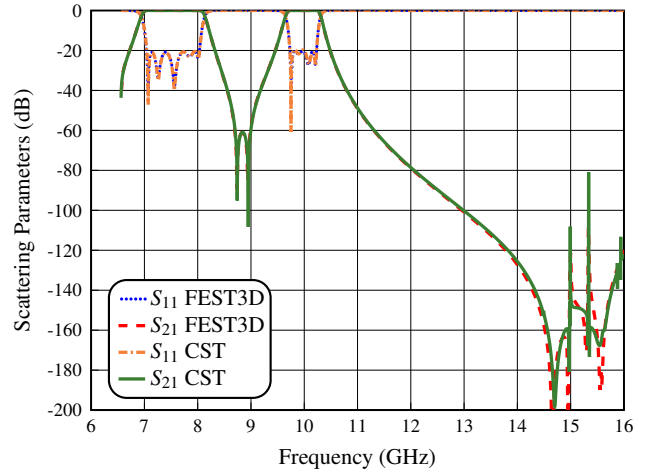


Fig. 27. Simulated performance of the dual band RA staircase filter with capacitive stubs before the input and output RAs using FEST3D and CST.

$RL_1 > 20$ dB; for the upper band the specifications are $f_2 = 10$ GHz, $BW_2 = 500$ MHz and $RL_2 > 20$ dB.

Additionally, the sharp corners of the distributed resonators have been changed into rounded corners with a radius $r_1 = 1.1$ mm and the capacitive stubs end with a radius equal to $r_2 = 1.0$ mm, in order to facilitate manufacturing. The resulting structure is shown in Fig. 26. Fig. 27 shows a comparison of the simulated behavior of the dual-band structure obtained with the commercial tools FEST3D and CST Studio Suite.

As we can see, the agreement is very good. Also, simulations show a very good out-of-band response, with spurious peaks below -80 dB from 12 to 16 GHz.

Table II shows the final values for all dimensions of the filter. The dimensions are given up to the center of the filter. This is because the filter is asymmetrical, but the central part of the filter is symmetrical. The thickness of the RAs is t_i , and the all capacitive stubs have the same width as the input waveguide.

TABLE II
PHYSICAL DIMENSIONS FOR THE DB RA STAIR TZ FILTER.

Section Type	Dimensions (mm)	
Input Waveguide	$a = 22.86$	
	$b = 10.16$	
	$L_{input} = L_{output} = 22.86$	
Capacitive stubs 1-2	$l_{cs_1} = 11.896$	$l_{cs_2} = 11.896$
	$t_{cs_1} = 2.0$	$t_{cs_2} = 2.0$
Capacitive stubs 3-4	$l_{cs_3} = 11.296$	$l_{cs_4} = 11.296$
	$t_{cs_3} = 2.0$	$t_{cs_4} = 2.0$
Resonant aperture 1-5	$a_1 = 22.616$	$a_5 = 22.720$
	$b_1 = 7.187$	$b_5 = 7.673$
	$t_1 = 3.974$	$t_5 = 4.005$
Resonator 1-4	$w_1 = 22.747$	$w_4 = 22.747$
	$H_1 = 11.432$	$H_4 = 11.432$
	$L_1 = 21.655$	$L_4 = 21.791$
Resonant aperture 2-4	$a_2 = 21.257$	$a_4 = 21.257$
	$b_2 = 2.771$	$b_4 = 2.771$
	$t_2 = 3.955$	$t_4 = 3.955$
Resonator 2-3	$w_2 = 22.424$	$w_3 = 22.424$
	$H_2 = 6.914$	$H_3 = 6.914$
	$L_2 = 22.074$	$L_3 = 22.074$
Resonant aperture 3	$a_3 = 20.823$	
	$b_3 = 1.326$	
	$t_3 = 4.003$	

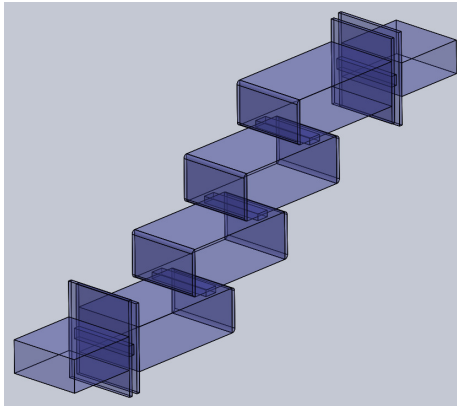


Fig. 28. Structure of the extended band pass RA filter with two stubs both before and after of the input and output RAs (EB RA Stair TZ Filter) designed with a radius equal to $r = 1.1$ mm in the distributed resonators.

B. Extended Band Pass RA Prototype

Next, we will design the EB RA stair TZ filter structure (see Fig. 24) with rounded corners. The specifications of the extended band pass RA filter are given in Table I. Also in this case, we have replaced all sharp concave corners with rounded corners with a radius equal to $r = 1.1$ mm, except on the capacitive stubs that are manufactured with spark erosion.

The final structure that we have obtained is shown in Fig. 28. Fig. 29 shows the comparison of the simulated performances obtained with FEST3D and CST. As we can see, the agreement is very good. In addition, the simulations show a very good out-of-band response, with spurious below -60 dB from 9 to

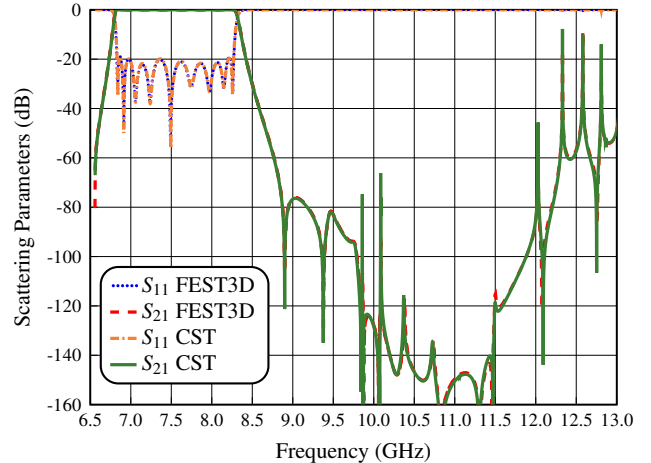


Fig. 29. Simulated performance of the extended band pass RA filter with two stubs both before and after of the input and output RAs (EB RA Stair TZ Filter) using FEST3D and CST.

TABLE III
PHYSICAL DIMENSIONS FOR THE EB RA STAIR TZ FILTER.

Section Type	Dimensions (mm)	
Input Waveguide	$a = 22.86$	
	$b = 10.16$	
	$L_{input} = L_{output} = 22.86$	
Capacitive stubs 1-2	$l_{cs_1} = 10.861$	$l_{cs_2} = 8.217$
	$t_{cs_1} = 1.1$	$t_{cs_2} = 1.1$
Capacitive stubs 3-4	$l_{cs_3} = 7.343$	$l_{cs_4} = 6.352$
	$t_{cs_3} = 1.1$	$t_{cs_4} = 1.1$
Capacitive stubs 5-6	$l_{cs_5} = 6.870$	$l_{cs_6} = 5.343$
	$t_{cs_5} = 1.1$	$t_{cs_6} = 1.1$
Capacitive stubs 7-8	$l_{cs_7} = 9.510$	$l_{cs_8} = 8.658$
	$t_{cs_7} = 1.1$	$t_{cs_8} = 1.1$
Resonant aperture 1-5	$a_1 = 20.814$	$a_5 = 20.814$
	$b_1 = 3.155$	$b_5 = 3.203$
	$t_1 = 2.0$	$t_5 = 2.0$
Resonator 1-4	$w_1 = 22.86$	$w_4 = 22.86$
	$H_1 = 13.550$	$H_4 = 13.550$
	$L_1 = 39.868$	$L_4 = 39.415$
Resonant aperture 2-4	$a_2 = 20.525$	$a_4 = 20.525$
	$b_2 = 4.095$	$b_4 = 4.095$
	$t_2 = 2.0$	$t_4 = 2.0$
Resonator 2-3	$w_2 = 22.86$	$w_3 = 22.86$
	$H_2 = 14.325$	$H_3 = 14.325$
	$L_2 = 39.633$	$L_3 = 39.633$
Resonant aperture 3	$a_3 = 20.392$	
	$b_3 = 3.857$	
	$t_3 = 2.0$	

12 GHz.

Table III shows the final values for all dimensions of the filter. The dimensions are given up to the center of the filter. This is because the filter is asymmetrical, but the central part of the filter is symmetrical. The thickness of the RAs is t_i , and all the resonators and capacitive stubs have the same width as the input waveguide.

TABLE IV
RESULTS OF THE TOLERANCE ANALYSIS FOR THE RA FILTERS.

Filter Type	Yield of the Structure			
Tolerance	5 μm	10 μm	15 μm	20 μm
DB RA Filter	98 %	92 %	70 %	40 %
EB RA Filter	78 %	54 %	38 %	14 %

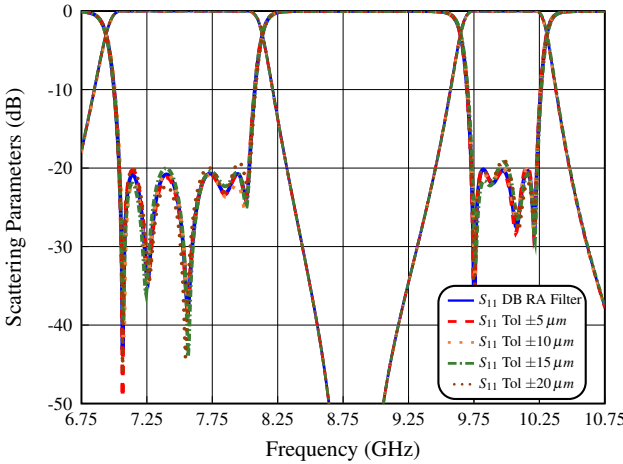


Fig. 30. Tolerance analysis of the dual band RA filter.

VI. YIELD ANALYSIS

In this section we show the results of a yield analysis for the RA filters that we have designed. For this purpose, we have used the commercial tool FEST3D to introduce a random error with a Gaussian distribution in the RA filters dimensions.

The sensitivity analysis for the RA filtering structures, have been carried out with different values of the standard deviation, namely, ± 5 , ± 10 , ± 15 and $\pm 20 \mu\text{m}$. Furthermore, since the filters have been designed with a return loss of 20 dB, the threshold value for the yield estimation has been set to 18 dB. Table IV shows a summary of the results obtained for the RA filters.

Figs. 30 and 31 show a number of simulations, including random errors for the RA filters. As we can see from both the simulations and the results in Table IV, with manufacturing errors between 5 and 10 μm , it should be possible to obtain an acceptable yield value. It is important to note that, although wide band filters are normally considered to be insensitive to manufacturing errors, our yield analysis does not reflect this point since manufacturing errors between 5 and 10 μm can be considered to be high accuracy manufacturing.

VII. HIGH POWER ANALYSIS

One of the most important features for space applications is the multipactor behavior of the filters [38]. In order to identify the power (Watts) where the multipactor effect can be initiated, a number of simulations have been carried out with our filter structures. The detailed procedure is fully described in [19], and will not be repeated here for the sake of space. Tables V and VI show the power thresholds that we have obtained for the dual band and extended band pass RA filters.

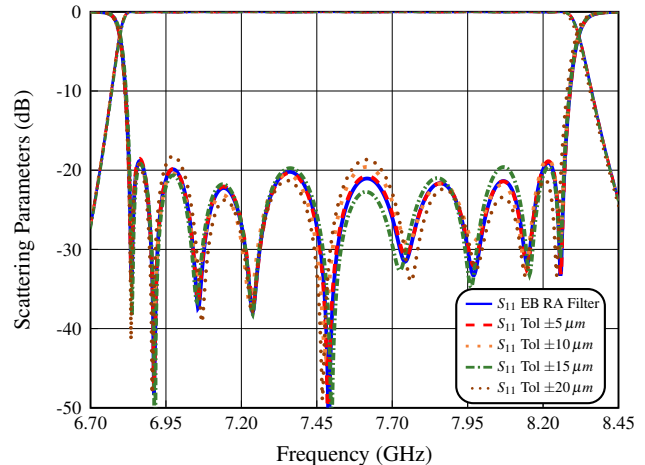


Fig. 31. Tolerance analysis of the extended band pass RA filter.

TABLE V
HIGH POWER ANALYSIS OF THE DUAL BAND RA FILTER.

Structure	Power of the structure		
Frequency	$f_1 = 6.97 \text{ GHz}$	$f_2 = 7.50 \text{ GHz}$	$f_3 = 8.11 \text{ GHz}$
$RA_2 = RA_4$	234 W	931 W	404 W
RA_3	113 W	284 W	185 W
Frequency	$f_4 = 9.68 \text{ GHz}$	$f_5 = 10.0 \text{ GHz}$	$f_6 = 10.29 \text{ GHz}$
$RA_2 = RA_4$	6749 W	3574 W	1137 W
RA_3	5249 W	1562 W	568 W

TABLE VI
HIGH POWER ANALYSIS OF THE EXTENDED BAND PASS RA FILTER.

Structure	Power of the structure		
Frequency	$f_1 = 6.81 \text{ GHz}$	$f_2 = 7.55 \text{ GHz}$	$f_3 = 8.30 \text{ GHz}$
RA_1	484 W	1875 W	1138 W
$RA_2 = RA_4$	195 W	1235 W	378 W
RA_3	204 W	1135 W	403 W
RA_5	1112 W	1887 W	2974 W

As expected, the resonant apertures (RA_3 and RA_2) show the lowest power threshold at 6.97 and 6.81 GHz with 113 and 195 W for the dual band and extended band pass RA filters, respectively. It is important to note that the multipactor power levels obtained are indeed remarkable considering the significant size reduction that we have been able to obtain with the proposed filter topologies.

To further evaluate the high power performance of the RA filters described in this contribution, we have designed a standard nine-pole symmetric capacitive filter. For this purpose, we have used the WR-112 waveguide in order to meet the same specifications given in Section IV. Table VII shows the final values for all dimensions of the structure.

The power thresholds that we have obtained for this last filter are shown in Table VIII. As expected, the capacitive window h_5 of the capacitive filter shows the lowest power threshold at 8.30 GHz with 2274 W. This power level is indeed higher than the power level allowed by our RA filter. However, the performance of the RA filter is remarkable if we take

TABLE VII
PHYSICAL DIMENSIONS FOR THE STANDARD CAPACITIVE FILTER.

Section Type	Dimensions (mm)
Input Waveguide	$a = 28.499$ $b = 12.624$
Capacitive window 1-10	Resonator 1-9
$h_1 = h_{10} = 8.017$	$L_1 = L_9 = 37.464$
$h_2 = h_9 = 5.716$	$L_2 = L_8 = 36.431$
$h_3 = h_8 = 4.423$	$L_3 = L_7 = 35.463$
$h_4 = h_7 = 3.809$	$L_4 = L_6 = 34.974$
$h_5 = h_6 = 3.546$	$L_5 = 34.816$

TABLE VIII
HIGH POWER ANALYSIS OF THE STANDARD NINE-POLE CAPACITIVE FILTER.

Structure	Power of the structure		
Frequency	$f_1 = 6.81$ GHz	$f_2 = 7.55$ GHz	$f_3 = 8.30$ GHz
h_5	35597 W	8449 W	2274 W

into account that it is about 60% shorter than the standard capacitive implementation.

VIII. MEASUREMENTS

The RA prototypes discussed in the previous sections have been manufactured in a clam shell configuration, using a combination of standard milling and spark erosion.

A. Dual Band RA Filter

The dual band RA staircase filter prototype is shown in Fig. 32. The comparison between measured and simulated in-band and out-of-band responses is shown in Fig. 33. To obtain the results in the stopband of the Fig. 33, we have used three standard waveguide calibrations, namely WR-90, WR-75 and WR-62, with the TRL (Through, Reflection and Line) method. The noise floor in each calibration was about -70 dB.

As we can see, the two passbands are centered at 7.5 and 10.0 GHz, respectively, the five and four reflection zeros of the dual band RA filter are clearly visible, and the agreement with the simulation is excellent.

There is also a good agreement between simulation and measurement in the out-of-band response, with spurious below

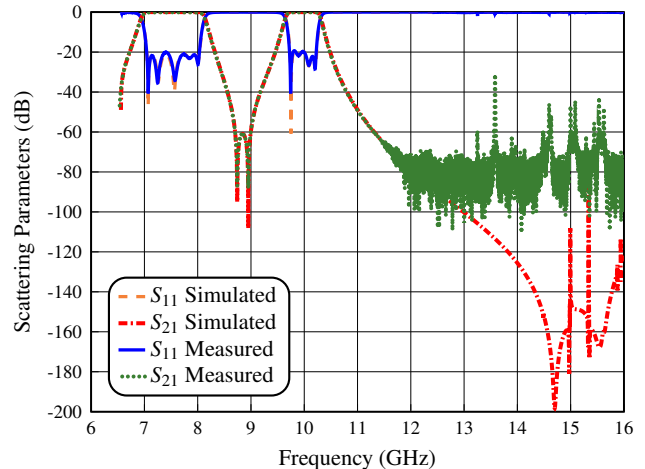


Fig. 33. Measurement of the in-band and out-of-band performance of the dual band RA filter compared with the EM simulation (CST).

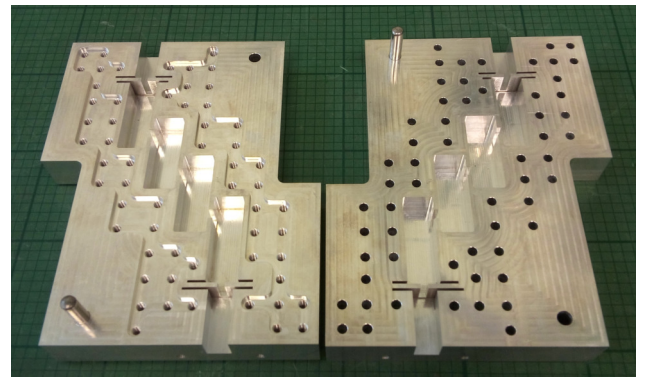


Fig. 34. Manufactured extended band pass RA prototype in aluminum (no silver plating).

-40 dB from 13 to 16 GHz. However, there is a spike reaching -30 dB at about 13.5 GHz. The spike is probably due to higher order mode excitation caused by manufacturing errors.

B. Extended Band Pass RA Filter

Next, we have manufactured the extended band pass RA filter, as shown in Fig. 34. The comparison between measured and simulated in-band and out-of-band responses are shown in Figs. 35 and 36, respectively.

As we can see, the in-band performance is centered at 7.55 GHz, the nine reflection zeros of the extended band pass RA filter are clearly visible, and the agreement with the simulation is excellent. There is also a good agreement between simulation and measurement in the out-of-band response, with spurious below -75 dB from 9 to 12 GHz, and -30 dB from 12 to 13 GHz with spikes reaching -35, -25 and 27.5 dB at about 12.33, 12.58 and 12.80 GHz, respectively.

It is interesting to note that a number of dips appears in the measured S_{11} results. To better understand this point we have simulated the filter including losses and, as we can see in Fig. 36, the same dips are now clearly visible. It is therefore apparent that the dips are due to power dissipated in the filter structure. To further investigate this point, we have computed

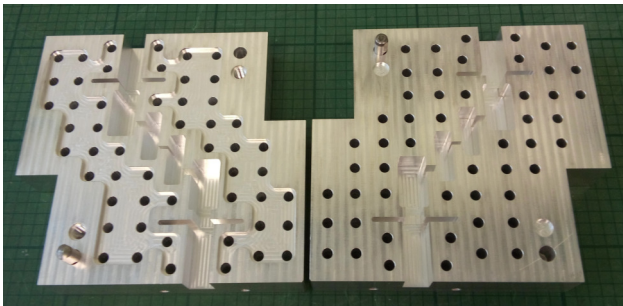


Fig. 32. Manufactured dual band RA prototype in aluminum (no silver plating).

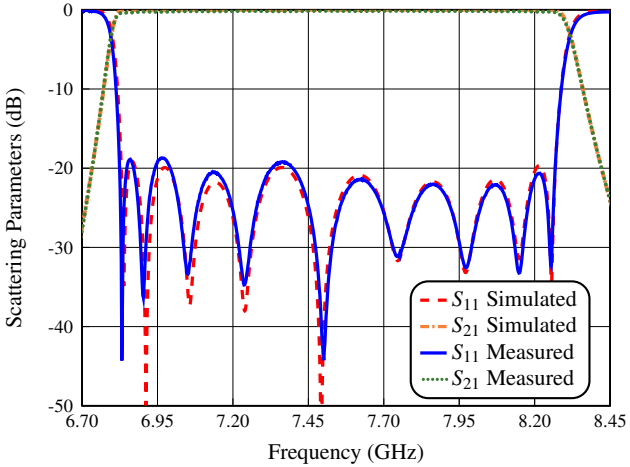


Fig. 35. Measurement of the in-band performance of the extended band pass RA filter compared with the EM simulation (CST).

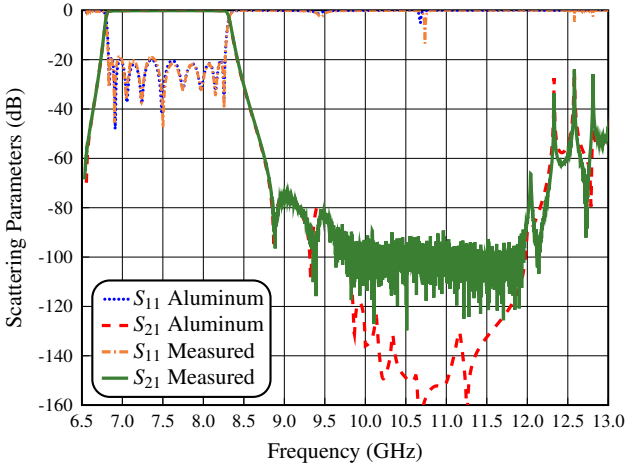


Fig. 36. Measurement of the out-of-band performance of the extended band pass RA filter compared with the EM simulation (CST) including losses due to the finite conductivity of the aluminum.

the fields inside the structure. The results obtained, not shown here for the sake of space, indicate that the dips are, in fact, due to resonances in some of the capacitive stubs used to introduce transmission zeros.

It is important to mention that the manufacturing error has been kept below $10 \mu\text{m}$ for all the curved corners, and below $5 \mu\text{m}$ for all other filter elements. The RA filter performances that have been obtained are indeed excellent, and are in full agreement with the results of the yield analysis that we performed.

IX. TECHNICAL DISCUSSION

In this section, we will discuss some of the technical aspects (or practical features) of the filters based on resonant apertures proposed in this paper.

A. Dual Band RA Filter Case

We discuss first some practical design aspects of the dual band RA filter.

The minimum and maximum bandwidths that can be achieved for the two pass bands of the in-line DB RA filter (see Fig. 10), if no TZs are present between the pass bands, turns out to be related to the rejection between the two bands. In our design we have obtained a rejection level of -14.5 dB . Increasing the bandwidth of the two pass bands, will reduce the rejection level, thereby degrading the inter-band response of the filter.

With this in mind, we can say that the minimum guard band (distance) between the two pass bands of the filter can be equal to zero (extended bandwidth case). While the maximum guard band depends on the individual filter pass bands, center frequencies, and the cut-off frequency of the main waveguide.

On the other hand, if we introduce TZs between the bands (as shown in Fig. 19) we have an additional constraint on the achievable guard band between the filters. This is because the presence of a TZ affects the coupling level of the resonant apertures. This in turn, poses a limitation to the minimum guard band that can be achieved.

This effect is due to the relation between the position of the TZs and the strength (height) of the coupling produced by the RAs when they function as coupling elements. In more detail, since the capacitive stub introduces a TZ, the closer is the TZ to the filter passband edge, the lower is the achieved coupling (for a given coupling aperture) and, as a consequence, the coupling window needs to be opened further. The limiting point is reached when the coupling window has the same height as the waveguide connected to the RA. This effect was, in fact, already noticed in [19]. To give a *rule of thumb* to estimate this effect, we have computed the following ratio:

$$\Delta TZ = \frac{BTZ}{BW} \quad (14)$$

where BTZ is the distance between the frequency of the TZs (below the pass band) and the lower edge of the pass band, and BW is the bandwidth of the filter. In [19] the ratio (14) is approximately equal to unity. Looking at the dual band response in Fig. 33, we can clearly see that the TZs between the two bands are approximately located at their respective limit (one filter bandwidth). As a consequence, for this filter, the guard band between the two pass bands cannot be made smaller.

Another issue that needs to be considered is that the staircase configuration implemented in the DB RA Filter, that shows an important improvement of the out-of-band response of the filter, does result in a limitation in the bandwidth of the second pass band that uses distributed resonators (BW_2 of Section V). The second band turns out to be smaller in comparison to the first band, due to the fact that the staircase geometry reduces the coupling between resonators. This is again due to the introduction of TZs in the filter transfer function. However, the first band is composed only of RAs and, therefore, the bandwidth is not affected by the staircase configuration.

Another point of interest is the achieved unloaded Q in the DB RA Stair TZ Filter. From the specifications of Section V, and the measured insertion loss performance shown in Section VIII, we have computed the unloaded Q using the

TABLE IX
UNLOADED Q OF THE RESONATORS OF THE DB RA STAIR FILTER.

Section Type	Insertion Loss (IL)	Unloaded Q
RAs	0.1725 dB	1415
RES	0.1615 dB	2995

TABLE X
PHYSICAL DIMENSIONS FOR THE HIGH-PASS FILTER.

Section Type	Dimensions (mm)
Input Waveguide	$a = 22.86$ $b = 10.16$ $L_{input} = 10$
Section 1	$w_1 = 18.788$ $h_1 = 10.16$ $L_1 = 9.057$
Section 2	$w_2 = 16.556$ $h_2 = 10.16$ $L_2 = 10.604$

procedure described in [39]. The results obtained are shown in Table IX. As we can see, the RAs have a Q value that is about half the Q value of the distributed resonators (RES).

Another important issue that needs to be discussed at this point is that the measured performances of our two prototypes have been obtained using only the fundamental TE_{10} mode excitation. To complete our investigation, we now study the performance of the DB RA Stair Filter under higher order modes excitation. In this context, however, only the TE_{20} higher order mode needs to be studied in detail.

As in [19], if the higher order modes are present in the excitation, we can easily suppress the spurious responses generated by the TE_{20} higher order mode using a simple high-pass filter at the output of our filter. Table X shows the final values for all dimensions of a high-pass filter that could be used in this context.

Fig. 37 shows the comparison of the simulated performances

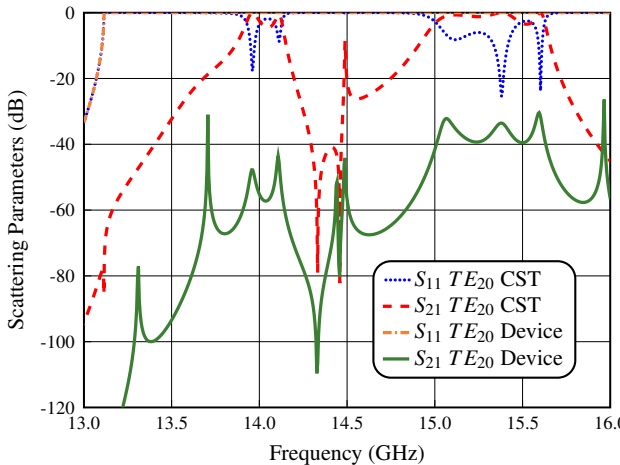


Fig. 37. Simulated performance (using CST) of dual band RA staircase filter with TE_{20} excitation (TE_{20} CST) compared to the performance of the filter plus high-pass device (TE_{20} Device).

TABLE XI
PHYSICAL DIMENSIONS FOR THE TRANSFORMER.

Section Type	Dimensions (mm)
Input Waveguide	$a = 25.959$ $b = 12.954$ $L_{input} = 10$
Section 1	$w_1 = 24.414$ $h_1 = 11.947$ $L_1 = 15.257$
Section 2	$w_2 = 23.328$ $h_2 = 11.000$ $L_2 = 21.248$

of the dual band RA filter (DB RA Stair TZ Filter) under higher order mode excitation, and the performance including the high-pass device. As we can see, we now have spurious responses below -30 dB from 13 to 16 GHz. This is indeed an important improvement.

B. Extended Band Pass RA Filter Case

Next, we discuss practical design aspects for the extended band pass RA filter. The minimum bandwidths of the pass band of the EB RA filters discussed in this paper, depend on a trade-off between the manufacturing process used to manufacture the filter, the dimensions of the structure, and the power requirements. The maximum bandwidth, on the other hand, depends on the limitations imposed by the staircase geometry. In our design we have tried to achieve the best trade-off between bandwidth of the pass band and rejection of the spurious resonances.

Another issue of relevance is the calculation of the unloaded Q in the EB RA Stair TZ Filter. From the specifications in Section IV, and the measured insertion value (0.1929 dB from results in Section VIII), we have computed an averaged Q-factor value ($Q=1986$) for the RAs and the distributed resonators [39].

The next issue that we discuss is the presence of higher order modes in the excitation. In this context, it is important to mention that our EB RA Stair TZ Filter is mono-modal until 13 GHz. For that reason, additional actions are not necessary with respect to the presence of higher order modes in the frequency range explored in this paper. However, if we increase the frequency up to 16 GHz, we will require the high-pass filter that we have already described, in order to suppress the higher order modes.

An additional issue that needs to be discussed is that the objective of our research is indeed to prove that RAs can effectively be used in filter design, however, our filter does not actually operate in the standard WR-90 waveguide range. This can be addressed in two ways. The first is to redesign the filters to operate with a higher center frequency. This is indeed possible, as shown in Fig. 4. The second is to add a small waveguide transformer to change the input of the filters to the WR-102 waveguide (see Fig. 38), so that the filter can operate in the standard WR-102 waveguide frequency range. Table XI shows the final values for all dimensions of the transformer.

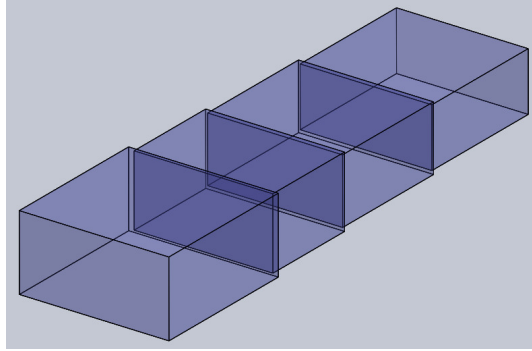


Fig. 38. Structure of the transformer composed of rectangular waveguide sections of smaller width and height.

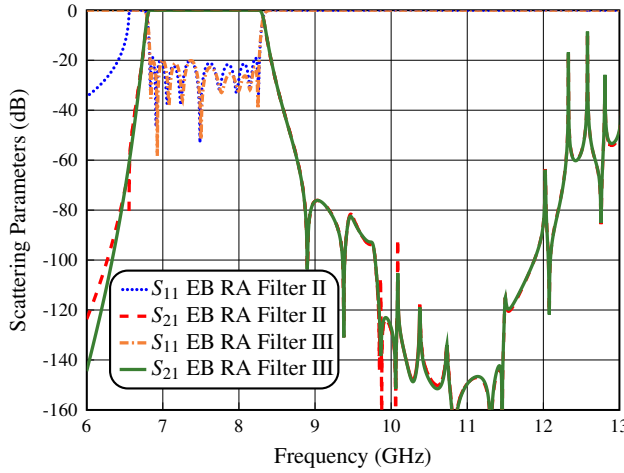


Fig. 39. Simulated performance of the EB RA Stair TZ Filter (EB RA Filter II), and the same filter implemented with the transformer at the input and output of the filter (EB RA Filter III).

To validate this last concept, we have compared the simulated performance of the EB RA Stair TZ Filter (EB RA Filter II) with the same filter with the addition of the transformer at the input and output of the filter (EB RA Filter III), as shown in Fig. 39. As we can see, the performance of the filter remains unchanged, and the operational bandwidth is now in the WR-102 range.

X. CONCLUSION

In this paper, we have provided the proof of concept of the feasibility of using resonant apertures (RAs) in the design of wide-band single and dual bandpass filters demonstrating a substantial reduction in filter length, good out-of-band response and improved selectivity. Furthermore, yield and multipaction analyses have also been carried out. In addition to theory, the measured performance of two prototypes has also been discussed indicating very good agreement with simulations, thereby fully validating the new family of filters that we propose and their design procedures.

REFERENCES

- [1] R.V. Snyder, "Filter design for modern communication systems," in *2012 Asia Pacific Microwave Conference Proceedings*, Dec. 2012, pp. 673–675.
- [2] R.V. Snyder, A. Mortazawi, I. Hunter, S. Bastioli, G. Macchiarella, and K. Wu, "Present and future trends in filters and multiplexers," *IEEE Trans. Microw. Theory Techn.*, vol. 63, no. 10, pp. 3324–3360, Oct. 2015.
- [3] R. Levy, R.V. Snyder, and G. Matthaei, "Design of microwave filters," *IEEE Trans. Microw. Theory Techn.*, vol. 50, no. 3, pp. 783–793, Mar. 2002.
- [4] I.C. Hunter, L. Billonet, B. Jarry, and P. Guillon, "Microwave filters—applications and technology," *IEEE Trans. Microw. Theory Techn.*, vol. 50, no. 3, pp. 794–805, Mar. 2002.
- [5] H. Wang, L. Zhu, and W. Menzel, "Ultra-wideband bandpass filter with hybrid microstrip/cpw structure," *IEEE Microw. Wireless Compon. Lett.*, vol. 15, no. 12, pp. 844–846, Dec. 2005.
- [6] T. Kuo, S. Lin, and C.H. Chen, "Compact ultra-wideband bandpass filters using composite microstrip–coplanar-waveguide structure," *IEEE Trans. Microw. Theory Techn.*, vol. 54, no. 10, pp. 3772–3778, Oct. 2006.
- [7] V. Bagheri, M. Mansouree, K. Mohammadpour-Aghdam, and R. Faraji-Dana, "Design, construction and measurement of a millimeter-wave filter with 40–60 GHz pass-band," in *2014 Third Conference on Millimeter-Wave and Terahertz Technologies (MMWATT)*, Dec. 2014, pp. 1–4.
- [8] G.L. Matthaei, L. Young, and E.M.T. Jones, *Microwave Filters, Impedance-Matching Networks, and Coupling Structures*. Norwood, MA: Artech House, 1980.
- [9] F.M. Vanin, D. Schmitt, and R. Levy, "Dimensional synthesis for wide-band waveguide filters," in *2004 IEEE MTT-S International Microwave Symposium Digest (IEEE Cat. No.04CH37535)*, vol. 2, Jun. 2004, pp. 463–466.
- [10] ———, "Dimensional synthesis for wide-band waveguide filters and diplexers," *IEEE Trans. Microw. Theory Techn.*, vol. 52, no. 11, pp. 2488–2495, Nov. 2004.
- [11] P. Soto, E. Tarín, V.E. Boria, C. Vicente, J. Gil, and B. Gimeno, "Accurate synthesis and design of wideband and inhomogeneous inductive waveguide filters," *IEEE Trans. Microw. Theory Techn.*, vol. 58, no. 8, pp. 2220–2230, Aug. 2010.
- [12] Q. Wu, F. Zhu, Y. Yang, and X. Shi, "An effective approach to suppressing the spurious mode in rectangular waveguide filters," *IEEE Microw. Wireless Compon. Lett.*, vol. 29, no. 11, pp. 703–705, Nov. 2019.
- [13] S. Li, J. Fu, and X. Wu, "Analysis of high-power rectangular waveguide filter with capacitive coupling iris for satellite," in *2009 Asia-Pacific Power and Energy Engineering Conference*, Mar. 2009, pp. 1–4.
- [14] ———, "Rectangular waveguide band pass filter with capacitive coupling iris," in *Progress in Electromagnetics Research Symposium 2008 (PIERS 2008)*, Mar. 2008, pp. 337–341.
- [15] J. Valencia, M. Guglielmi, S. Cogollos, J. Vague, and V.E. Boria, "Enhancing the performance of stepped impedance resonator filters in rectangular waveguide," in *2017 47th European Microwave Conference (EuMC)*, Oct. 2017, pp. 989–992.
- [16] J. Valencia, V.E. Boria, M. Guglielmi, and S. Cogollos, "Compact wideband hybrid filters in rectangular waveguide with enhanced out-of-band response," *IEEE Trans. Microw. Theory Techn.*, vol. 68, no. 1, pp. 87–101, Jan. 2020.
- [17] C. Carceller, P. Soto, V.E. Boria, and M. Guglielmi, "Capacitive obstacle realizing multiple transmission zeros for in-line rectangular waveguide filters," *IEEE Microw. Wireless Compon. Lett.*, vol. 26, no. 10, pp. 795–797, Oct. 2016.
- [18] J. Valencia, M. Guglielmi, S. Cogollos, and V.E. Boria, "Enhancing the out-of-band response of hybrid wide-band filters in rectangular waveguide," in *2020 50th European Microwave Conference (EuMC)*, Jan. 2021, pp. 747–750.
- [19] J.F. Valencia Sullca, M. Guglielmi, S. Cogollos, and V.E. Boria, "Hybrid wideband staircase filters in rectangular waveguide with enhanced out-of-band response," *IEEE Trans. Microw. Theory Techn.*, vol. 69, no. 8, pp. 3783–3796, Aug. 2021.
- [20] F. Arndt, T. Duschak, U. Papziner, and P. Rolappe, "Asymmetric iris coupled cavity filters with stopband poles," in *IEEE International Digest on Microwave Symposium*, vol. 1, May 1990, pp. 215–218.
- [21] F. Arndt and T. Sieverding, "The rigorous CAD of aperture-coupled T-junction bandstop-filters, E-plane circuit elliptic-function filters, and diplexers," in *1991 IEEE MTT-S International Microwave Symposium Digest*, vol. 3, Jul. 1991, pp. 1103–1106.
- [22] T. Sieverding and F. Arndt, "Field theoretical CAD of open or aperture matched T-junction coupled rectangular waveguide structures," *IEEE Trans. Microw. Theory Techn.*, vol. 40, no. 2, pp. 353–362, Feb. 1992.

- [23] U. Rosenberg, S. Amari, and J. Bornemann, "Mixed-resonance compact in-line pseudo-elliptic filters," in *IEEE MTT-S International Microwave Symposium Digest*, 2003, vol. 1, Jun. 2003, pp. 479–482.
- [24] ——, "Inline TM₁₁₀-mode filters with high-design flexibility by utilizing bypass couplings of nonresonating TE_{10/01} modes," *IEEE Trans. Microw. Theory Techn.*, vol. 51, no. 6, pp. 1735–1742, Jun. 2003.
- [25] U. Rosenberg, S. Amari, J. Bornemann, and R. Vahldieck, "Compact pseudo-highpass filters formed by cavity and iris resonators," in *2004 34th European Microwave Conference (EuMC)*, vol. 2, Oct. 2004, pp. 985–988.
- [26] T.S. Chen, "Characteristics of waveguide resonant-iris filters (correspondence)," *IEEE Trans. Microw. Theory Techn.*, vol. 15, no. 4, pp. 260–262, Apr. 1967.
- [27] M. Piloni, R. Ravenelli, and M. Guglielmi, "Resonant aperture filters in rectangular waveguide," in *1999 IEEE MTT-S International Microwave Symposium Digest (Cat. No.99CH36282)*, vol. 3, Jun. 1999, pp. 911–914.
- [28] M. Capurso, M. Piloni, and M. Guglielmi, "Resonant aperture filters: Improved out-of-band rejection and size reduction," in *2001 31st European Microwave Conference (EuMC)*, Sep. 2001, pp. 1–4.
- [29] Y. Wu, Q. Zeng, and Y. Shang, "A low-insert loss and high-return loss bandpass filter based on cut-off rectangular waveguide for satellite communication application," *International Journal of RF and Microwave Computer-Aided Engineering*, vol. 31, no. 2, pp. 1–8, Feb. 2021.
- [30] R. Barrio-Garrido, S. Llorente-Romano, and M. Salazar-Palma, "Design of Ka-band highly selective wideband band-pass filters using directly coupled resonant irises," in *IEEE Antennas and Propagation Society International Symposium. Digest. Held in conjunction with: USNC/CNC/URSI North American Radio Sci. Meeting (Cat. No.03CH37450)*, vol. 2, Jun. 2003, pp. 1161–1164.
- [31] R. Barrio-Garrido, S. Llorente-Romano, A. Garcia-Lamperez, and M. Salazar-Palma, "Design of broadband directly coupled non-centred resonant irises filters," in *2003 33rd European Microwave Conference (EuMC)*, Oct. 2003, pp. 219–222.
- [32] R. Barrio-Garrido, S. Llorente-Romano, M. Salazar-Palma, A. Onoro-Navarro, and I. Hidalgo-Carpintero, "Design, construction and experimental characterization of a broadband highly selective filter in waveguide technology in Ka-band," in *2006 IEEE MTT-S International Microwave Symposium Digest*, Jun. 2006, pp. 250–253.
- [33] C. Zong-tao and L. Sheng-xian, "Design of microwave filter with resonant irises of resonant windows at different location," in *2011 IEEE International Conference on Microwave Technology Computational Electromagnetics*, May 2011, pp. 156–159.
- [34] J.F. Valencia Sulca, S. Cogollos, M. Guglielmi, and V.E. Boria, "Dual-band filters in rectangular waveguide based on resonant apertures," in *2021 IEEE MTT-S International Microwave Symposium (IMS)*, Jun. 2021, pp. 192–195.
- [35] N. Marcuvitz, *Waveguide Handbook*, ser. IEE Electromagnetic Waves Series, vol. 21. Stevenage, UK: Peter Peregrinus Ltd., 1986.
- [36] D. M. Pozar, *Microwave Engineering*. John Wiley & Sons, 2012.
- [37] G. Conciario, M. Guglielmi, and R. Sorrentino, *Advanced Modal Analysis*. Wiley, 2000.
- [38] E. Sorolla *et al.*, "An analytical model to evaluate the radiated power spectrum of a multipactor discharge in a parallel-plate region," *IEEE Trans. Electron Devices*, vol. 55, no. 8, pp. 2252–2258, Aug. 2008.
- [39] I. Hunter, *Theory and Design of Microwave Filters*. IET Electromagnetic Wave Series 48, 2001.



Joaquin F. Valencia Sulca was born in Lima, Peru, on March 14, 1990. He received the Ingeniero de Telecomunicaciones degree from the Universidad Nacional de Ingeniería (UNI), Lima, Peru, in 2013, the master degree in communication technologies, systems and networks from the Universitat Politècnica de València, Valencia, Spain, in 2016, where he is currently pursuing the Ph.D. degree in telecommunications with the iTEAM Group. His current research interests include the analysis and design of passive components, electromagnetic simulations, efficient design and optimizations of waveguide filters, and its applications.



Santiago Cogollos was born in Valencia, Spain, on January 15, 1972. He received the Ingeniero Superior de Telecomunicación and Doctor Ingeniero de Telecomunicación degrees from the Universitat Politècnica de València (UPV), Valencia, Spain, in 1996 and 2002, respectively. In 2000 he joined the Communications Department of the Universitat Politècnica de València, where he was an Assistant Lecturer from 2000 to 2001, a Lecturer from 2001 to 2002, and became an Associate Professor in 2002. He has collaborated with the European Space Research and Technology Centre of the European Space Agency in the development of modal analysis tools for payload systems in satellites. In 2005 he held a post doctoral research position working in the area of new synthesis techniques in filter design at University of Waterloo, Waterloo, Ont., Canada. His current research interests include applied electromagnetics, mathematical methods for electromagnetic theory, analytical and numerical methods for the analysis of microwave structures, and design of waveguide components for space applications.



Vicente E. Boria (S'91-A'99-SM'02-F'18) was born in Valencia, Spain, on May 18, 1970. He received his "Ingeniero de Telecomunicación" degree (with first-class honors) and the "Doctor Ingeniero de Telecomunicación" degree from the Universidad Politécnica de Valencia, Valencia, Spain, in 1993 and 1997, respectively. In 1993 he joined the "Departamento de Comunicaciones", Universidad Politécnica de Valencia, where he has been Full Professor since 2003. In 1995 and 1996, he was holding a Spanish Trainee position with the European Space Research and Technology Centre, European Space Agency (ESTEC-ESA), Noordwijk, The Netherlands, where he was involved in the area of EM analysis and design of passive waveguide devices. He has authored or co-authored 10 chapters in technical textbooks, 180 papers in refereed international technical journals, and over 200 papers in international conference proceedings. His current research interests are focused on the analysis and automated design of passive components, left-handed and periodic structures, as well as on the simulation and measurement of power effects in passive waveguide systems. Dr. Boria has been a member of the IEEE Microwave Theory and Techniques Society (IEEE MTT-S) and the IEEE Antennas and Propagation Society (IEEE AP-S) since 1992. He is also member of the European Microwave Association (EuMA), and has been the Chair of the 48th European Microwave Conference held in Madrid, Spain. He acts as a regular reviewer of the most relevant IEEE and IET technical journals on his areas of interest. He has been Associate Editor of IEEE Microwave and Wireless Components Letters (2013–2018) and IET Electronics Letters (2015–2018). Presently, he serves as Subject Editor (Microwaves) of IET Electronics Letters, and as Editorial Board member of International Journal of RF and Microwave Computer-Aided Engineering. He is also member of the Technical Committees of the IEEE-MTT International Microwave Symposium and of the European Microwave Conference.



Marco Guglielmi was born in Rome, Italy, on December 17, 1954. He received the degree “Laurea in Ingegneria Elettronica” in 1979 from the University of Rome “La Sapienza”, Rome, Italy, where in 1980 he also attended the “Scuola di Specializzazione in Elettromagnetismo Applicato”. In 1981 he was awarded a Fulbright Scholarship in Rome, Italy, and an HISP (Halsey International Scholarship Programme) from the University of Bridgeport, Bridgeport, Connecticut, USA, where in 1982 he obtained an MS Degree in Electrical Engineering. In 1986

he received a PhD degree in Electrophysics from the Polytechnic University, Brooklyn, New York, USA. From 1984 to 1986 he was Academic Associate at Polytechnic University, and from 1986 to 1988 he was Assistant Professor in the same institution. From 1988 to 1989 he was Assistant Professor at the New Jersey Institute of Technology, Newark, New Jersey, USA. In 1989 he joined the European Space Agency as a Senior Microwave Engineer in the RF System Division of the European Space Research and Technology Centre (ESTEC), Noordwijk, The Netherlands, where he was in charge of the development of microwave filters and electromagnetic simulation tools. In 2001 he was appointed Head of the Technology Strategy Section of ESTEC where he contributed to the development of management processes and tools for the formulation of a European strategy for Space Technology Research and Development. In 2014 Dr. Guglielmi retired from the European Space Agency and is currently holding the position of Invited Senior Researcher at the Polytechnic University of Valencia, Valencia, Spain. Dr. Guglielmi has been elevated to the grade of Fellow of the IEEE in January 2013 “For contributions to multimode equivalent networks and microwave filter design”.